Energy Technology
Generation, Conversion, Storage, Distribution
www.entechnol.de

ZeoPTES: Zeotropic Pumped Thermal Energy Storage with an Ammonia–Water Mixture as Working Fluid

Aiko Bernehed

The rapid rise of renewable energy production necessitates the development of large-scale electricity storage systems. Pumped thermal energy storage (PTES), where electricity is stored in hot and cold storage units, has recently garnered a lot of interest. Previously proposed PTES systems rely on pure fluids as working fluids in Brayton- or Rankine-based power cycles. Herein, ZeoPTES, a PTES system using a zeotropic mixture of ammonia and water as working fluid, is introduced. The mixture exhibits nonisothermal evaporation and condensation, which allows utilization of industrially available sensible storage units, like water or molten salt, to store the thermal energy from these phase changes. A simulation using the REFPROP 10.0 database is written to analyze the cycle. Eight parameters are identified as having an effect on system round-trip efficiency and 30 000 simulations with random values for these parameters are run to identify the impact of all. Although efficient compressors and expanders are necessary to reach a high power-to-power round-trip efficiency, the largest system-wide losses arise from entropy generation and thermal stream mismatch in the cold and hot side heat exchangers. Using state-of-the-art microchannel heat exchangers with extremely low pinch points allows for round-trip efficiencies in excess of 70%.

1. Introduction

With the rapid rise of electricity production from renewable sources with varying power input, low-cost, and long-term storage systems are gaining importance. The International Energy Agency estimates an additional 310 GW of power output from storage systems is required in the USA, Europe, China, and India, by 2050.[1] Currently, about 173 GW of energy storage technologies are operational worldwide, of which 96,6% are pumped hydro storage (PHS).[2] Although PHS is an interesting technology with widespread benefits, further successful deployment of PHS at large scale is questionable, as projects require long lead times, need to fulfill specific geographic requirements, and can face backlash from community stakeholders due to significant local environmental impact.[3] As an alternative to PHS a wide variety of mechanical, chemical, thermal, and electrical energy storage technologies are currently being considered, comprehensive overviews of which are provided by Rahman et al.[4] and Benato and Stoppato.[5]

1.1. Pumped Thermal Energy Storage

One emerging storage technology of particular interest is pumped thermal energy storage (PTES),[5] which uses a heat pump to store electrical energy as heat in thermal storage tanks. At a later time, the stored heat can be used to generate electricity via a conventional power cycle.[6] The technology uses mature power plant machinery and has a theoretical round-trip efficiency limit (power-to-power) of 100%.[7,8] PTES systems can be categorized according to the thermal cycle used in their design. Desrues et al.[9] designed a system with turbomachines in a Brayton cycle. In charging mode, the authors heat a working gas isentropically with a compressor and transfer the resulting heat to a storage tank filled with refractory material. The cold, pressurized gas is then expanded through a turbine after which it subsequently gets heated back up by extracting heat from a "cold" storage tank, thus completing the work cycle. In discharge mode the system operates in reverse with a different set of turbine and compressor. Macnaghten and Howes[10] from Isentropic Ltd. designed a similar system using a custom-made reciprocating engine. Laughlin[8] uses four turbomachines and external liquid thermal storage tanks with molten salt in the hot and a hydrocarbon cryogen in the cold-side storage tanks. All Brayton cycles found in the literature solely use sensible heat storage units. Davenne and Peters[11] provide a thorough loss analysis of Brayton PTES systems and conclude that the isentropic expander efficiency has the highest influence on the system's round-trip efficiency. For a hypothetical 1 GWh storage unit, the authors present an estimated round-trip efficiency of 60–65%.

In contrast, Mercangöz et al.[12] proposed a system with carbon dioxide (CO_2) as the working fluid in a Rankine cycle, which the authors call eectrothermal energy storage (ETES). The CO_2 is in a transcritical state on the system's hot side, which leads to excellent matching of the thermal profile with the external heat storage tanks, and in a subcritical state on the cold side. Therefore, the cold-side storage is characterized by an isothermal phase change (PC), i.e., boiling and condensing, which requires a latent heat storage system. The authors propose to use a series of pressurized water tanks as hot side and one water-ice unit as cold-side

A. Bernehed
Institute of Solar Research
German Aerospace Center
Prof.-Rehm-Str. 1, 52428 Jülich, Germany
E-mail: aiko.bernehed@dlr.de

The ORCID identification number(s) for the author(s) of this article can be found under https://doi.org/10.1002/ente.202100470.

DOI: 10.1002/ente.202100470

storage. Several different hot storage tanks with varying flow rates are necessary to provide a close match of the thermal profiles of the working and storage fluid to one another.[13] Kim et al.[14] developed a strong argument for the importance of having a small back work ratio in the storage system. The back work ratio is defined as the ratio of the expander-to-compressor work ratio in charge and the compressor-to-expander work ratio in discharge mode. The authors explain that a small back work ratio leads to lower entropy generation in the working machines and therefore to a higher round-trip efficiency. As the compressor in a Brayton gas power cycle can consume as much as 2/3 of the turbine work, one can expect PTES systems with Rankine cycles with fluid pumps to be more efficient. Kim et al.[14] expand on the ETES system by replacing the isentropic compressor and expander with isothermal machines, thus decreasing the back work ratio and achieving a 3.3 percentage-points higher round-trip efficiency. Steinmann[15] developed the compressed heat energy storage (CHEST) concept, which uses water as a working fluid. The compressor is a multistep machine with integrated intercooling to achieve temperatures of 350–400 °C at an upper pressure of 105 bar. The cycle also uses a bottoming ammonia cycle during the charging stage to provide the necessary temperature required to boil the working fluid before compression. Hot side thermal energy is stored in a latent heat storage unit where steam condensation occurs and in sensible storage tanks where the working fluid is exclusively liquid or gaseous. The mean hot side storage temperature is comparatively high, which leads to a higher efficiency of the discharge heat engine and smaller thermal storage tanks. In fact, Steinmann et al.[16] argue that a higher mean temperature is advantageous for low exergy losses and therefore higher round-trip efficiency. The authors also present simulation results for a variety of different storage technologies and parameter variations and show that the CHEST system is a competitive choice.

Subsequently, this work led to the development of the ORC-CHEST by Jockenhöfer et al.,[17] which uses an organic working fluid, requires only a single-stage compression, and uses no ammonia bottoming cycle. All CHEST-based cycles work at subcritical pressures and use a combination of sensible and latent heat storage material on the hot side and water or the environment on the cold side. Hassan et al.[18] and Eppinger et al.[19] recently independently investigated a variety of different working fluids for ORC–Rankine-based PTES systems. Eppinger et al.[20] further developed their technology and proposed an experimental implementation, which is currently in commissioning. In contrast to CHEST, their system uses only one hot water storage tank and does not require a latent heat thermal storage unit. While this potentially leads to lower storage cost, the poor thermal match between the storage and working fluid may increase exergy losses, thus reducing the system's round-trip efficiency. Steinmann et al.[21] and Jockenhöfer et al.[17] also showed multiple ways how an ORC–CHEST system could be integrated with low-temperature heat sources to provide electricity storage and local district heating services. Using low-temperature heat that would otherwise be dumped to the environment may open up further revenue streams to the system operator and provide a competitive advantage. The interested reader is referred to Dumont et al.,[22] who compiled a comprehensive overview of proposals for PTES systems.

1.2. Ammonia–Water Working Fluid

To develop a PTES system with a high round-trip efficiency and low investment and operating cost, the advantages of Brayton and Rankine cycle-based systems need to be combined while mitigating their respective disadvantages. Such a system requires a high back work ratio, a high mean temperature, and low-cost storage units. In this work, ZeoPTES, a PTES system with a zeotropic mixture of ammonia and water as working fluid in a Rankine cycle is presented. Zeotropic mixtures have interesting properties, because in contrast to pure substances, they display a temperature glide during evaporation and condensation.[23,24] Therefore, these mixtures facilitate a better matching of the external heat source temperature profile, e.g., hot gas-turbine exhaust gases, to the temperature profile of the working fluid.

ZeoPTES combines the respective advantages of the previously discussed Brayton and Rankine cycles, and particularly benefits from a low back work ratio. As the condensation and evaporation of the working fluid is not isothermal, cost-efficient sensible heat storage systems that are common place in industry today can be utilized. With careful matching of the storage and working fluid mass flow rate, a close temperature match and, thus, a high heat exchanger efficiency can be realized. Ammonia and water both exhibit high critical pressures and temperatures, and therefore facilitate the design of a subcritical Rankine cycle with an elevated mean temperature. Furthermore, the system only uses one compression and one expansion unit on the gas side, minimizing losses from nonisentropic state changes as they occur in the cold-side machines in Brayton PTES systems.

Although to date, no PTES system using a zeotropic mixture as working fluid has been reported, there is previous work from the power industry to build on. In 1984, Kalina[25] was the first to propose the use of a zeotropic mixture of ammonia and water as a working fluid for power generation units. In 1987, design planning on a 3 MW demonstration facility at Canoga Park, California commenced.[26] The unit used a 70/30 ammonia–water mixture at temperatures and pressures up to 510 °C and 110 bar during regular operation, whereas the ceiling temperature was limited by the turbine specifications. According to Leibowitz and Mirolli,[27] the power plant operated successfully for 5200 h between 1992 and 1995. The authors also report an estimated yearly loss of 0.11 to 1.76% of working fluid at temperatures between 900 and 980 °F (482–527 °C). Based on these results, ZeoPTES ceiling temperatures should be limited to reduce the amount of working fluid lost. Today the cycle is frequently used for low temperature geothermal power generation[28] and is studied for high-temperature applications in concentrated solar power plants.[29]

The model underlying the ZeoPTES system and the simulation to calculate its charge and discharge cycle, and round-trip efficiency is introduced in Section 2. In Section 3, the results of several parameter variations are discussed. Furthermore, simulations of 30 000 random values of a specified parameter set were carried out and the results presented here. Section 4 concludes this work and provides an outlook to future research.

2. System Modeling

ZeoPTES uses a zeotropic mixture of ammonia and water as working fluid in a subcritical power cycle. The potential cycle layout of a storage plant is shown in **Figure 1**. The system uses a Rankine cycle for charging and discharging, which minimizes the back work ratio. A corresponding *T*–*s* diagram is shown in **Figure 2**. In charging mode, starting at point 1 (Figure 1a), an electrically driven compressor raises the working fluid pressure and temperature (1 → 2). The fluid's thermal energy is subsequently transferred to thermal storage units via heat exchangers. Here, the system is divided into working fluid gas cooling (2 → 3), condensation (3 → 4), and liquid subcooling (4 → 5). The now cold working fluid is then expanded in a throttle (5 → 6). Finally, the working fluid is evaporated in a final heat exchanger (6 → 1) using thermal energy stored from the last discharging cycle, thus closing the cycle.

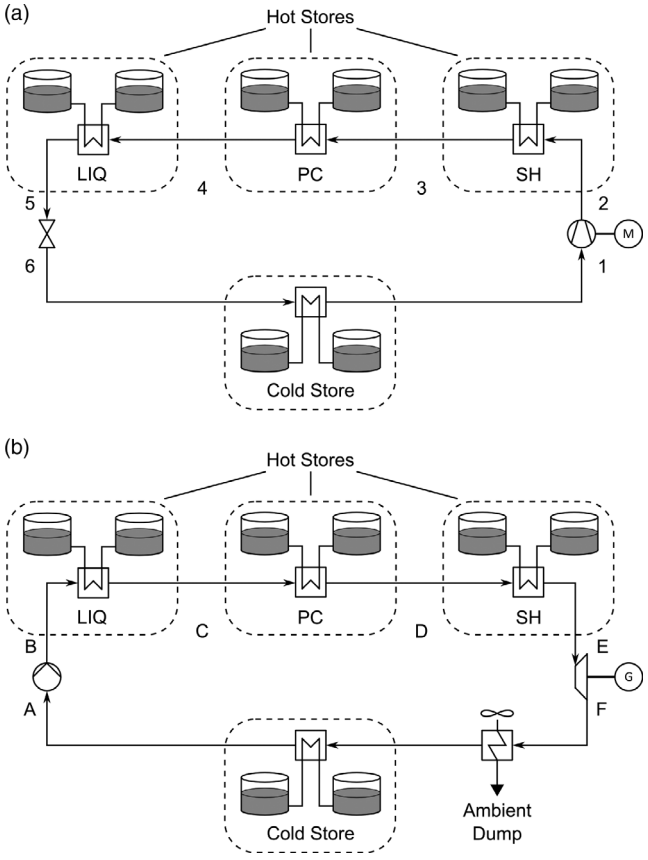

Figure 1. Presented are the basic layouts for the a) charge and b) discharge cycle of the ZeoPTES concept. Both cycles use the same hot and cold storage tanks and heat exchangers, but different working machines. The hot side storage systems are divided into the three parts, which represent the liquid (LIQ), phase change (PC), and superheating (SH) regime of the working fluid. The charge cycle follows the direction 1 → 2 → 3 → 4 → 5 → 6 → 1. The discharge cycle runs in reverse at slightly different pressures and temperatures in the cycle A → B → C → D → E → F → A. The discharge cycle also contains an ambient dump before the cold storage system, which is used to remove excess entropy from the storage system.

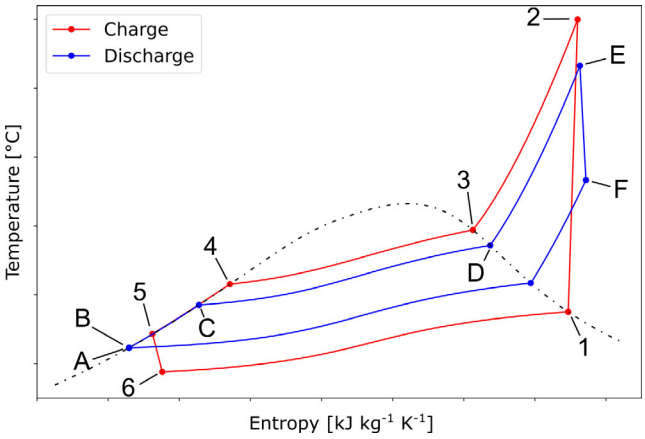

Figure 2. *T*–*s* diagram of an example cycle.

In discharging mode (Figure 1b), the liquid working fluid's pressure is raised by a pump (A→B), with subsequent heating (B→C), evaporation (C→D), and superheating (D→E). The now hot and pressurized working fluid is then expanded in a turbine (E→F), which drives a generator to produce electricity again. The depressurized, warm working fluid is finally passed into the final heat exchanger for cooling and condensation (F → A). The thermal energy stream from (F → A) carries all surplus entropy generated in both cycles due to irreversibilities, and exceeds the energy required by the storage cycle in (6→1). This low-temperature surplus thermal energy needs to be removed from the system, which is achieved here by dumping thermal energy to ambient air.

Due to the working fluid's temperature glide during evaporation and condensation, liquid sensible storage material can be used in all storage units, potentially reducing their cost. Different storage materials may be necessary at different points in the cycle, depending on the temperature level. At temperatures below 200 °C, water in pressurized vessels may be used. At higher temperatures, heat transfer fluids commonly used in concentrated solar power plants, like synthetic oils and molten salt mixtures, can be used.[30,31] The exact state of the working fluid in each point can be controlled with control strategies similar to those used in conventional power plants. The working fluid mass stream in charging and discharging mode are set by providing the appropriate power to the charge compressor and working fluid pump. Ceiling pressures are controlled by altering the open flow areas of the charge throttle and discharge turbine valves. Finally, the energy added and removed from each cycle step is controlled by altering the storage medium mass flow via the appropriate auxiliary pump. These latter pumps and a necessary working fluid holding tank on the liquid side are not shown in Figure 1. To change between the charging and discharging modes the storage medium flow is reversed and three-way valves, also not shown, are used to switch between the charging and discharging machinery shown in Figure 1. The exact layout of every piece of machinery and the design of control strategies are an interesting feat of engineering and need to be investigated further in future work.

2.1. Round-Trip Efficiency

The round-trip efficiency of the entire storage system is defined as the power-to-power electrical efficiency between the charge (CH) and the discharge (DI) cycles

$$\eta_{\text{round}} = \frac{E_{\text{DI}}}{E_{\text{CH}}} \tag{1}$$

where E_{CH} and E_{DI} denote the total electrical energy charged into and discharged out of the storage system. Ignoring losses in generators and motors, these can be calculated as

$$E_{\text{CH}} = \dot{m}_{\text{CH}}\,\tau_{\text{CH}}\left|\sum w_{\text{CH}}\right| \tag{2}$$

$$E_{\text{DI}} = \dot{m}_{\text{DI}}\,\tau_{\text{DI}}\left|\sum w_{\text{DI}}\right| \tag{3}$$

This notation allows for different charging and discharging time frames τ_i using different mass flows $\dot{m}_i$ during charging and discharging. All thermal–mechanical energy conversions in turbines, compressors, and pumps are captured in the different w_i. For a full charge and discharge cycle to complete, the hot storage system completely charges and discharges a fixed amount of thermal energy $Q_{\text{hot}} = Q_{\text{hot,CH}} = Q_{\text{hot,DI}}$. Thus, we obtain

$$\dot{m}_{\text{CH}}\,\tau_{\text{CH}}\,q_{\text{hot,CH}} = Q_{\text{hot}} = \dot{m}_{\text{DI}}\,\tau_{\text{DI}}\,q_{\text{hot,DI}} \tag{4}$$

with thermal streams q_i. Substitution in Equation (1) then leads to

$$\eta_{\text{round}} = \frac{q_{\text{hot,CH}}}{q_{\text{hot,DI}}} \cdot \frac{\left|\sum w_{\text{DI}}\right|}{\left|\sum w_{\text{CH}}\right|} \tag{5}$$

In the aforementioned case, the cold storage system only stores as much energy during discharge as is needed to facilitate the PC from 6→1 during the charge cycle, i.e., $Q_{\text{cold,DI}} = Q_{\text{cold,CH}}$. As described earlier, excess energy needs to be removed such that $Q_{\text{F}\to\text{A}} = Q_{\text{cold,DI}} + Q_{\text{Ambient Dump}}$. It should be noted that it is theoretically possible for the cold storage system to generate too little thermal energy for the charge cycle, such that the hot storage system cannot fully discharge. In such a case, the ambient dump needs to be moved so the hot storage tanks can be regenerated for the next charge cycle. This impacts Equation (4) and (5) to change in the following way

$$\dot{m}_{\text{CH}}\,\tau_{\text{CH}}\,q_{\text{cold,CH}} = Q_{\text{cold}} = \dot{m}_{\text{DI}}\,\tau_{\text{DI}}\,q_{\text{cold,DI}} \tag{6}$$

$$\eta_{\text{round}} = \frac{q_{\text{cold,CH}}}{q_{\text{cold,DI}}} \cdot \frac{\left|\sum w_{\text{DI}}\right|}{\left|\sum w_{\text{CH}}\right|} \tag{7}$$

In general though, the former case holds and the discharge working fluid stream carries enough thermal energy to charge the cold side storage system with excess being dumped to ambient. Therefore, Equations (4) and (5) apply. The exact characteristic of the charge and discharge thermal streams is further explored with the help of grand composite curves in Section 3.1.

2.2. Machines

Working machines used for expansion and compression can be categorized into turbomachinery and reciprocating machinery. Desrues et al.[9] and Laughlin[8] cite existing turbomachinery from industry, whereas Steinmann[15] presented an entirely new concept for an intercooled compressor. In contrast, Howes[32] and Willich and White[33] focus on custom designed piston engines for their energy storage concepts. The advantages and disadvantages of different types of working machines in PTES systems will be investigated in future research. In this work however, a fixed isentropic efficiency η_i is chosen without any further consideration of the machines' types and operating characteristics. The specific compressor and expander work then calculate as

$$w_{\text{Comp.}} = \frac{h_{\text{out,id.}} - h_{\text{in}}}{\eta_{\text{Comp.}}} \tag{8}$$

$$w_{\text{Exp.}} = \eta_{\text{Exp.}} \cdot (h_{\text{in}} - h_{\text{out,id.}}) \tag{9}$$

where $h_{\text{out,id.}}$ would be the state reached with an ideal isentropic compression or expansion and h_{out} is the state actually reached. The remaining enthalpy difference between h_{out} and $h_{\text{out,id}}$ is irreversibly converted into entropy and needs to be removed from the system.

The charge cycle consists of a gas-side compressor and a fluid-side expander. The expander can either be a working machine that returns mechanical energy to the compressor or a simple throttle. In the latter case, the simulation uses an isentropic efficiency of $\eta_{\text{CH,exp.}} = 0$ which leads to $h_{\text{exp.,in}} = h_{\text{exp.,out}}$, i.e., no enthalpy conversion in the throttle. Due to entropy production in the throttle, the round-trip efficiency is nevertheless reduced. The efficiency loss due to the use of a throttle in contrast to a mechanical expander is investigated in Section 3.3. The discharge cycle consists of a liquid pump on the fluid and an expander on the gas side. To allow better comparability with other storage concepts, losses from motors and generators are not considered here.

2.3. Storage Systems and Heat Exchangers

Different PTES concepts rely on different thermal energy storage units. Desrues et al., Howes, and White and Parks[9,32,34] use Brayton gas cycles, where the gas flows through a solid sensible storage material like crushed rock. The direct contact of the working fluid with the storage material leads to excellent storage efficiency, but the thermal fronts in the storage unit tend to decay over time, which lowers efficiency.[35] Mercangöz et al.[12] used pressurized water as a storage material on the hot and latent heat ice storage on the cold side of their ETES system. Laughlin[8] envisioned molten salt used in concentrated solar power plants today[36] as hot side and liquid cryogenic hydrocarbons as cold-side thermal storage units, with industrial heat exchangers used to transfer thermal energy between the working and storage fluids.

Liquid storage substances have the advantage that they can be pumped from one storage vessel through a counter-flow heat exchanger into another vessel, bypassing the decay of thermal fronts as they occur in solid storage materials.[35] Therefore,

a much closer temperature approach between the storage and working fluid is possible, minimizing entropy generation in the heat exchanger. The layouts for the hot and cold side storage systems are shown in **Figure 3** and **4**. On the hot side, the system is split into three different regimes, liquid (LIQ), PC, and superheating (SH), which correspond to the different phases that the working fluid is in while interacting with the storage material. Each section of storage uses a sensible storage material, whereas the temperature profile, i.e., the rise of the temperature for a given enthalpy change, is controlled by altering the mass flow of the storage material. Here, one can also see the benefits of using a zeotropic working fluid: as the working fluid does not have an isothermal PC as a pure fluid does, the thermal profile of the sensible storage material of the PC tanks can be closely matched to the thermal profile of the working fluid. Thermal profiles of pure fluids can only be closely matched during the PCs by using latent heat storage systems, which have an isothermal thermal profile as is proposed by Jockenhöfer et al.[17] As the proposed PTES system has no isothermal state changes, only sensible storage systems are considered.

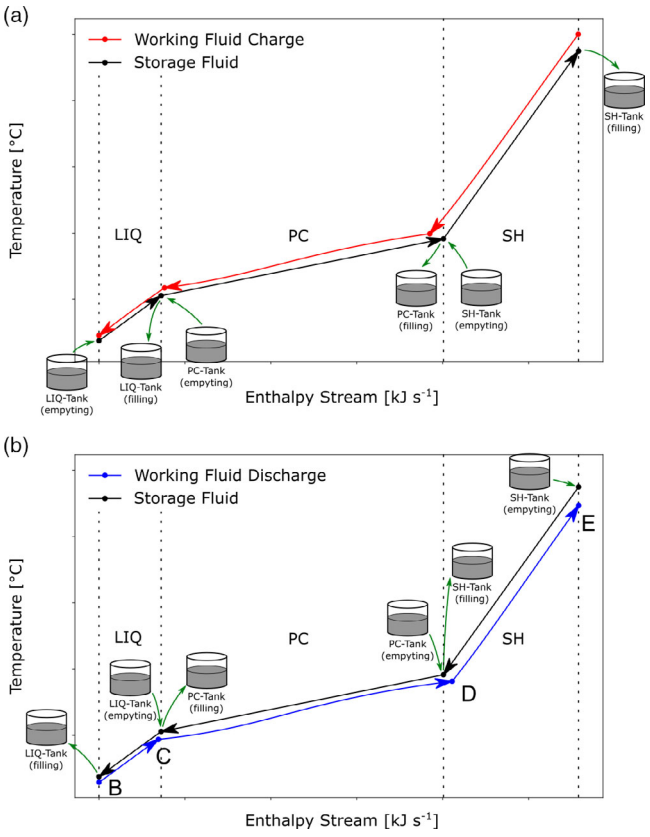

Figure 3. These illustrations depict how the thermal energy from the working fluid is stored in the sensible thermal storage tanks during a) charging and b) discharging. The three regimes (LIQ, PC, and SH) correspond to the three parts of same name in Figure 1 and represent the parts of the storage system where the working fluid is in an LIQ, PC, or SH state. Each regime is covered by different sensible energy storage materials, which is engineered to work within the required temperature range. For instance, colder parts could be covered by pressurized and unpressurized water storage tanks, whereas hotter parts require thermal oils or molten salts.

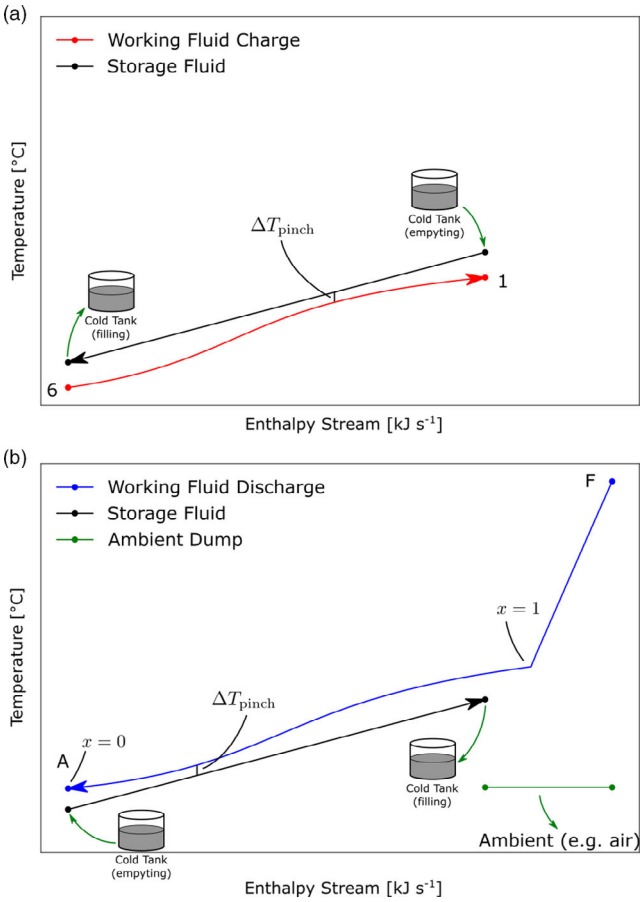

Figure 4. These illustrations show how the cold side thermal storage system works during a) charging and b) discharging. The discharge working fluid line has a sharp turn on the hot end, as the working fluid exits the discharge turbine in a superheated state and needs to be isobarically cooled down to the steam bell ($x = 1$) before undergoing condensation ($x = 0$). Excess entropy generated from irreversible state changes in working machinery and heat exchangers is removed during discharging via an ambient dump. Also depicted here are the closest temperature approaches that can be achieved between the working and storage fluids, which are determined by the heat exchanger pinch point ΔT_{pinch}.

On the cold side (Figure 4), the storage system works in reverse. The system gets charged with thermal energy during the discharging cycle, thereby allowing condensation of the working fluid to take place, and gets discharged during the storage system charge cycle. Also shown in Figure 4b is the ambient dump depicted in Figure 1b, which is assumed here to use the ambient air as a heat dump. Conceivably, this additional thermal energy could be used by industry in downstream applications. Furthermore, Figure 4 shows how the storage and working fluid thermal streams can diverge from one another. According to Baehr and Kabelac,[37] the rate of irreversible entropy generation in an infinitesmal section of a heat exchanger can be derived as

$$\mathrm{d}\dot{S}_{\text{irr}} = \frac{T_{\text{hot}} - T_{\text{cold}}}{T_{\text{hot}} \cdot T_{\text{cold}}} \mathrm{d}\dot{Q} \tag{10}$$

where the infinitesmal thermal energy stream $\mathrm{d}\dot{Q}$ flows from the hot to the cold stream. This means, that the temperature difference $\Delta T = T_{\mathrm{hot}} - T_{\mathrm{cold}} \geq \Delta T_{\mathrm{pinch}}$ should be kept as small as possible for every part of the heat exchanger. The pinch point temperature $\Delta T_{\mathrm{pinch}}$ is the closest temperature approach the heat exchanger was designed for. Smaller pinch points can be achieved at the expense of larger heat exchange areas, which typically entail larger heat exchange volumes and therefore increased investment and operating costs.

As shown in Figure 4, the temperature glide during cold-side evaporation and condensation (6→1 and F → A) is not linear, but shows a strong curvature due to changing mass fractions of ammonia and water in the gas and fluid phase. This leads to a change in the heat capacity of the mixture. Mercangöz et al.[12] faced a similar issue with the changing heat capacity of carbon dioxide on the transcritical side of ETES. The authors solved this problem by introducing auxiliary storage tanks between the two main tanks, which allow alteration of the storage fluid mass flow through the heat exchanger. In this work, a similar approach is pursued, as is shown in **Figure 5**. These auxiliary tanks are smaller than the main tanks at each end of the storage system and alter the mass flow by providing more mass or extracting some mass from the storage fluid mass stream. This leads to a much closer approach of the charge and discharge curve to the storage stream, as illustrated by $\Delta T_{\mathrm{pinch}}$ being hit multiple times, thus reducing entropy generation, as calculated by Equation (10). As Morandin et al.[38,39] illustrated, the exact behavior of the working fluid during charging and discharging, and the storage fluid thermal streams can be best explored using grand composite curves. In Section 3.1, a similar approach is used to discuss the impact the different amounts of storage units on the hot and cold side have on the entire system.

Instead of a two-tank storage system a single-tank thermocline unit with hot and cold storage fluid separation can also be used. Instead of setting specific storage materials at different state changes in the charge and discharge cycle, the simulation assumes each storage material to have a constant heat capacity. The storage fluid mass flow is adjusted to fit the thermal profiles of the storage and working fluids to one another. Currently, shell-and-tube heat exchangers with a temperature approach $\Delta T \approx 10\,\mathrm{K}$ are standard in the power industry, but plate, microchannel, and printed circuit heat exchangers provide a much closer temperature approach of down to $\Delta T_{\mathrm{pinch}} = 3\,\mathrm{K}$ at potentially lower cost.[40] As shown in Equation (10), a smaller pinch point, and therefore, a closer temperature approach, lead to less entropy generation in the heat exchangers. The pressure drop in the heat exchangers depends on the type of unit chosen, their geometry, and the volume, mass flow, temperature and pressure of the incoming working fluid. Pra et al.[40] investigated printed circuit heat exchanger designs for a recuperator in modular high temperature nuclear reactors and claim pressure losses between 27.9 and 70 kPa. For simplicity, a constant pressure drop of 30 kPa was chosen for this simulation. This is clearly an aggressive, yet feasible, estimate and the effect of the pressure drop on cycle performance will be further investigated in Section 3.3. Future work will consider a more detailed analysis of each heat exchanger used.

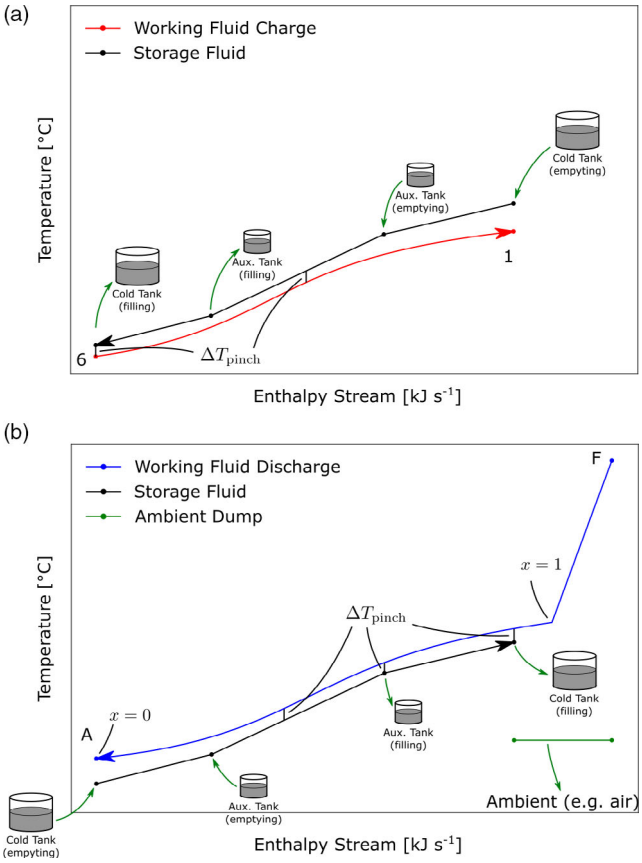

Figure 5. In these illustrations, the cold-side storage system is augmented by two auxiliary storage tanks. The simulation automatically iterates the configuration of these tanks to calculate the setup with the lowest entropy generation for a) charging and b) discharging, thus optimizing for round-trip efficiency. The heat exchanger is brought much closer to their pinch point, i.e., the minimum temperature difference they were engineered to allow between the two mass streams. These auxiliary storage systems allow a much closer approach of the thermal streams to one-another than the system without auxiliary tanks, as shown in Figure 4.

2.4. Simulation

The simulation is written in Python 3.8 using the ammonia–water equations of state from NIST REFPROP 10.0.[41,42] The caller provides starting values for the ammonia and water mass fraction $[x_{\mathrm{NH_3}}, x_{\mathrm{H_2O}}]$, desired ceiling temperature T_{hot}, charge cycle background pressure p_{back}, heat exchanger pinch point temperature difference $\Delta T_{\mathrm{pinch}}$, the amount of hot and cold storage tanks n_{hot} and n_{cold}, and the isentropic efficiencies of all four working machines $\eta_{\mathrm{CH,Comp.}}$, $\eta_{\mathrm{CH,Exp.}}$, $\eta_{\mathrm{DI,Pump}}$ and $\eta_{\mathrm{DI,Exp.}}$ during charging (CH) and discharging (DI). The simulation then follows the pattern shown in **Figure 6**. During execution, all necessary state changes and the grand composite curves are calculated. The caller receives data points for the calculated pressure p, temperature T, specific enthalpy h, specific entropy s, steam quality q, and density d during both cycles. The coefficient-of-performance $\mathrm{COP_{CH}}$ of the charge cycle, the power cycle efficiency η_{DI} of the discharge cycle, and the total round-trip efficiency of the storage

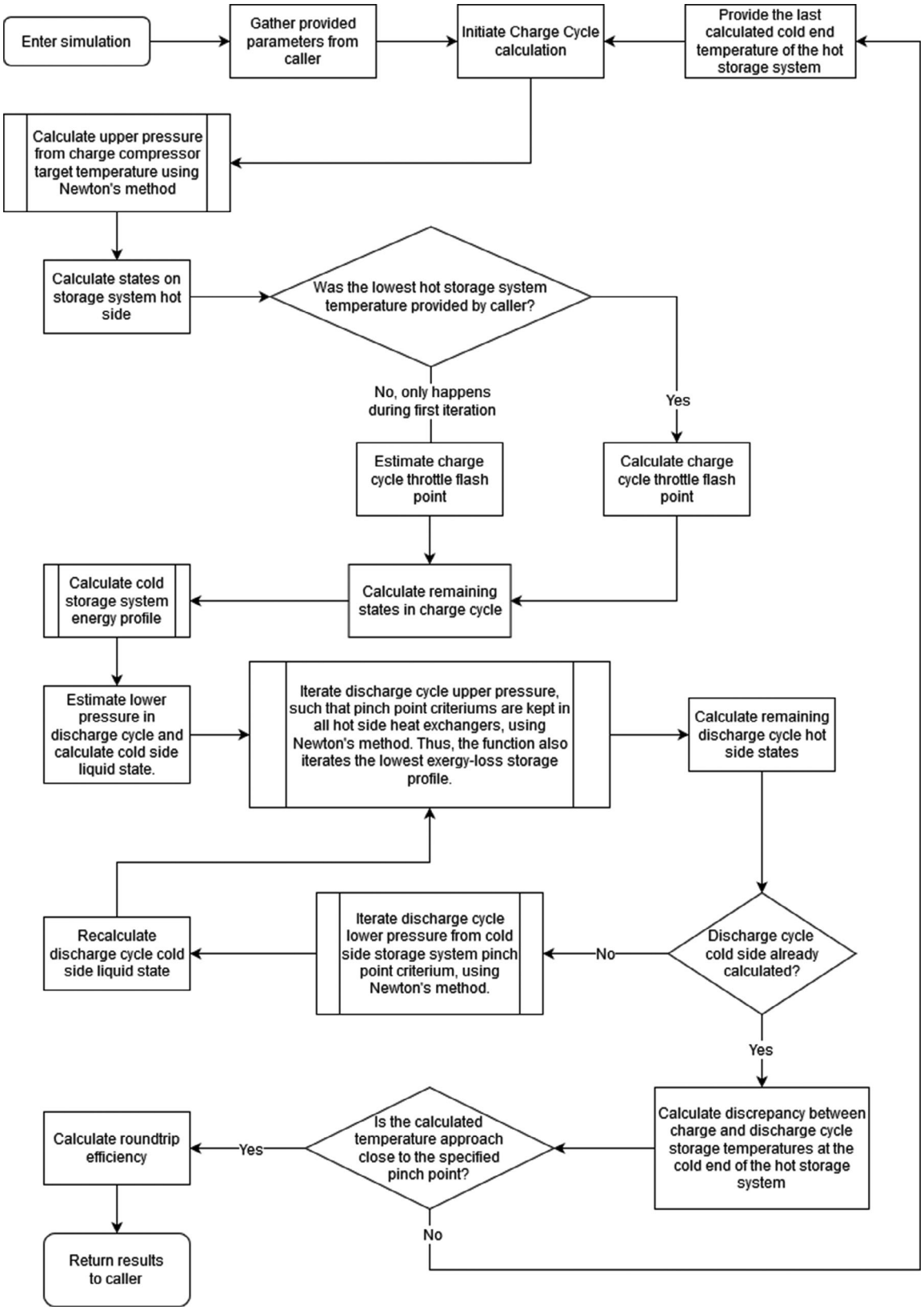

Figure 6. Core simulation flowchart for ZeoPTES.

system η_{round} are also provided. Furthermore, the grand composite curves are returned for subsequent analysis by the user.

3. Results and Discussion

The simulation was executed with a range of different parameter sets. The machine efficiencies for the charge compressor, discharge turbine, and discharge pump were set to $\eta_i = 0.9$. The charge expander was set to $\eta_{\text{CH,Exp.}} = 0$ to simulate a real throttle with no mechanical energy conversion. Except where otherwise noted, the heat exchanger pressure loss and pinch point temperature difference were chosen as constant with values $\Delta p = 30\,\text{kPa}$ and $\Delta T_{\text{pinch}} = 3\,\text{K}$, respectively. These values are aggressive, but achievable with current state-of-the-art printed circuit heat exchangers. The charge back pressure of the simulation was set to $p_{\text{back}} = 1.15\,\text{bar}$. This scheme is used to prevent ambient air from entering the system and contaminating the working fluid. With adequate sealing lower back pressures can also be implemented. The charge cycle ceiling temperature T_{hot} was varied between 400 and 500 °C. The ammonia mass fraction x_{NH_3} was kept between 10% and 90%. Unfortunately, REFPROP 10.0 exhibited significant convergence issues for values below 10% and above 90%. In regimes with such a lean mixture, the temperature glide is also not very pronounced, which reduces the benefits of using low-cost sensible storage materials over latent heat storage technology. For analysis of these outlying regimes other material databases need to be considered in the future. The amount of cold side auxiliary storage units $n_{\text{aux,cold}}$ was varied between zero and two. In Section 3.3, the effect of an even larger number of auxiliary tanks is investigated.

3.1. Grand Composite Curves

To analyze the effect of ΔT_{pinch} and the amount of cold-side auxiliary storage tanks $(n_{\text{aux,cold}})$, grand composite curves were used. These curves show the enthalpy streams $\dot{H}_i$ in the heat exchanger network and their temperature levels. In this work, the curves are split into cold and hot side energy streams to aid readability. In **Figure 7**, the hot side curves for a storage system ceiling temperature $T_{\text{hot}} = 500\,°\text{C}$ are displayed. The storage system thermal stream (black) is optimally fitted to the charge cycle thermal stream (red), while still ensuring that the pinch point condition is not violated. In turn, the discharge stream (blue) is fitted to the storage system stream (black). Therefore, the pinch point temperature approach ΔT_{pinch} directly influences the maximum achievable pressure and temperature of the discharge cycle in front of the turbine inlet (point E).

The temperature approach for the liquid regime (LIQ) between the charge cycle (4→5) and the discharge cycle (B→C) is only limited by the achievable heat exchanger pinch point ΔT_{pinch}. For the two-phase regime (PC), the discharge cycle pump pressure is adjusted such that the pressure is maximized while still meeting the pinch point criterion. The gas-side superheating stage (SH) is limited by the user-requested ceiling temperature T_{hot} for the charge cycle. The discharge cycle ceiling enthalpy is then calculated such that the discharge cycle cannot extract more total enthalpy than the charge cycle provided, i.e., $\dot{H}_2 = \dot{H}_{\text{E}}$ with $\dot{H}_5 = \dot{H}_{\text{B}}$ in Figure 7. The achieved ceiling temperature in point E is subsequently calculated from the pressure and enthalpy.

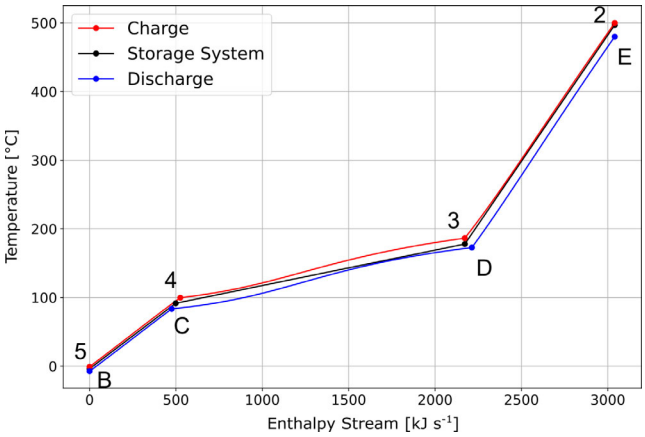

Figure 7. The hot side enthalpy streams with a temperature approach of $\Delta T_{\text{pinch}} = 3\,\text{K}$. The closer the charging and discharging lines approach the less entropy is generated, which leads to a higher round-trip efficiency. As can be seen here, the curvature of the enthalpy streams in the two-phase regime between (3→4, red) and (C→D, blue) limit this approach. Therefore, the discharge stream pressure is chosen such that the evaporation temperatures do not violate ΔT_{pinch}. This in turn determines the maximum temperature achievable in point E.

In contrast, **Figure 8** shows the thermal streams on the storage system cold side. The working fluid exits the discharge expander in a gaseous state and needs to be cooled before condensation begins. As previously pointed out, the amount of enthalpy released during discharging in (F → A) far exceeds the thermal energy required during subsequent charge cycle boiling (6→1). The surplus energy is low-temperature heat and can be used in local industry or district heating, or dumped to the environment. The charge cycle thermal profile is given by the user-requested back pressure p_{back} of the system. The discharge back pressure is then calculated such that it is minimized, while still meeting the pinch point criterion. More cold-side auxiliary storage systems lead to a better thermal matching between the charge and discharge thermal streams and thus a lower discharge back pressure, which in turn allows for a lower expander outlet temperature in point F (see axis in Figure 8a,b). The effect of the amount of auxiliary storage systems on the cold side on the storage system's round-trip efficiency is further discussed in Section 3.2 and 3.3.

These grand composite curves implicitly assume that the storage system mass flow is equal for the charge and discharge cycle, which is advantageous for a direct comparison of the thermal streams of both. This does not need to be the case. A different storage fluid mass flow for charge and discharge mode allows for a decoupling of the charging and discharging time spans τ_i the storage system can provide. Furthermore, these curves do not reflect thermal losses occurring in the piping and tanks during operations and downtime. They do, however, consider a pressure loss of $\Delta p = 30\,\text{kPa}$ in the working fluid side of each heat exchanger.

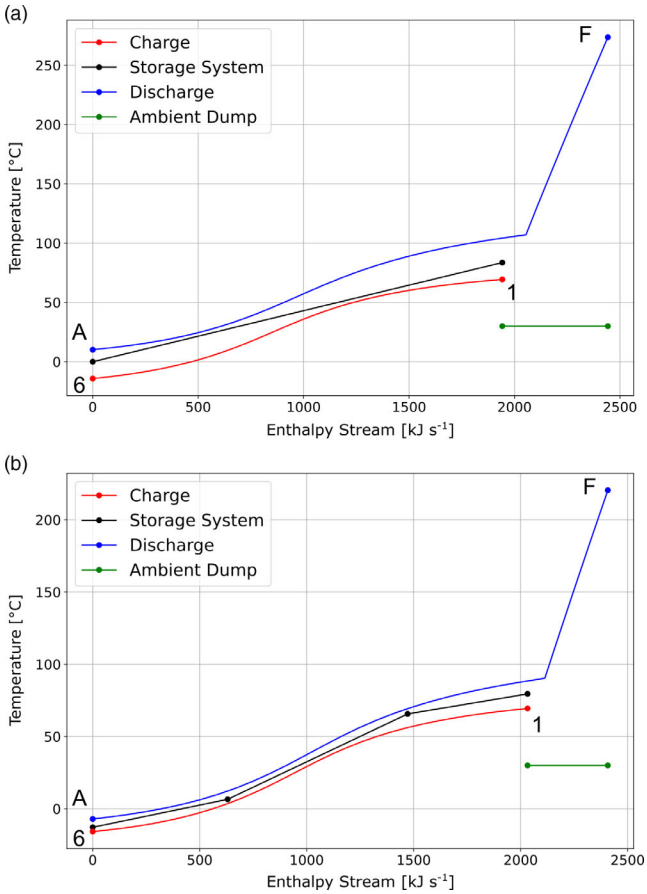

Figure 8. Cold side enthalpy streams with a) no and b) two auxiliary storage systems and the same pinch point temperature approach $\Delta T_{\text{pinch}} = 3$ K. The excess thermal energy resulting from irreversibilities in the storage system need to be removed from the system. Here, the energy is dumped to ambient, but use by industry is also a viable option that may open another revenue stream for the storage system operator.

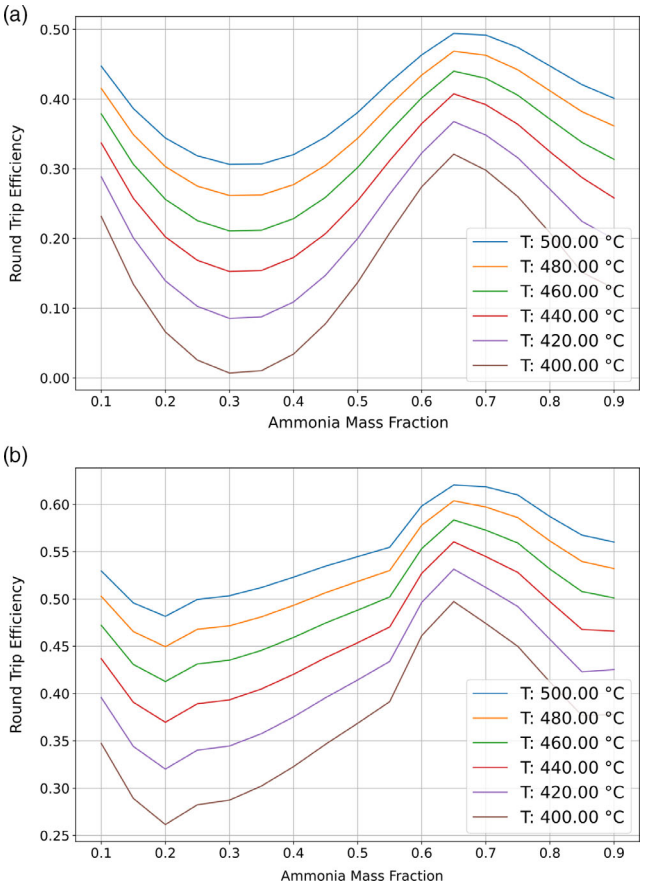

Figure 9. Round-trip efficiency η_{round} for a) no and b) two auxiliary storage systems $n_{\text{aux,cold}}$, a range of ceiling temperatures T_{hot}, varying ammonia mass fractions x_{NH_3}, and a constant back pressure of $p_{\text{back}} = 1.15$ bar. The use of more auxiliary storage systems yields a much higher round-trip efficiency, which results from the closer temperature approach between the charge and discharge cycle during evaporation and condensation.

3.2. Round-Trip Efficiency by Ceiling Temperature and Working Fluid Composition

The temperature glide and the boiling and condensing temperatures at the given back pressure p_{back} are influenced by the mass fractions of ammonia and water. In **Figure 9**, the round-trip efficiency is plotted against the ammonia mass fraction x_{NH_3} for different ceiling temperatures T_{hot}. The two graphs compare the influence of the amount of cold-side auxiliary storage tanks in the two-phase regime. Figure 9a shows the relationship for $n_{\text{aux,cold}} = 0$, Figure 9b for $n_{\text{aux,cold}} = 2$. Unsurprisingly, in both cases, higher temperatures lead to a higher round-trip efficiency. In both graphs, the maximum round-trip efficiency is exhibited at $x_{\text{NH}_3} = 0.65$ for every temperature. To understand this behavior, the evolution of the working fluid's heat capacity in relationship to the fluid's enthalpy for different ammonia mass fractions and an upper pressure of 60 bar is shown in **Figure 10**, defined here as

$$c_p = \left(\frac{\mathrm{d}h}{\mathrm{d}T}\right)_{p=\text{const.}} \tag{11}$$

Note that this equation does not work for pure fluid PCs, as $\mathrm{d}T = 0$ for isothermal state changes and c_p is therefore undefined. For the two-phase regime, a strong curvature develops, which is smallest for about $x_{\text{NH}_3} = 0.65$. The smaller this curvature is, the smaller the temperature difference is between the working fluid and the storage material thermal streams. Per Equation (10), this translates to a smaller entropy generation and therefore to a larger round-trip efficiency. The benefit of increasing the amount of cold-side auxiliary storage tanks $n_{\text{aux,cold}}$ is explained in Section 3.1. Here, one can see that choosing $n_{\text{aux,cold}} = 2$ can increase the round-trip efficiency by up to 13 percentage points.

To illustrate how different working fluid compositions, x_{NH_3} and different amount of cold storage units $n_{\text{aux,cold}}$ impact various cycle parameters and the working fluid behavior in the T–s diagram, three different cases are investigated. The input

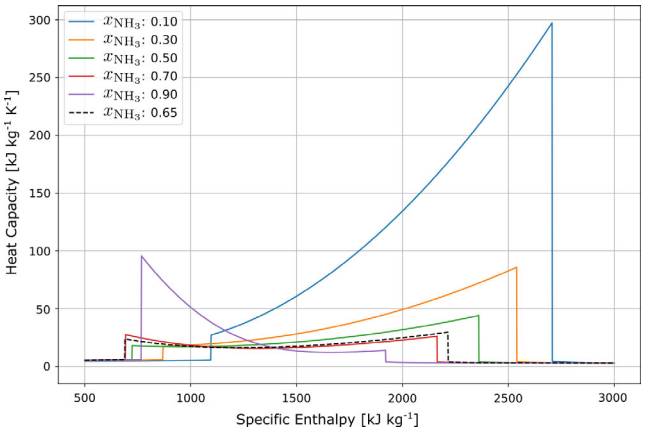

Figure 10. Displayed is the heat capacity of a working fluid mixture against the fluid's enthalpy for different working fluid compositions at 60 bar. The liquid (left) and gaseous (right) have a nearly constant heat capacity. During the two-phase regime the curves are wildly diverging though, which corresponds to a strong curvature of the working fluid thermal in the grand composite curves. The more constant the heat capacity of the working fluid is, the better it can be matched to a sensible storage material stream, which is assumed to have constant or near-constant heat capacity.

Table 1. The three presented cases only differ in the ammonia mass fraction and the amount of cold-side auxiliary storage systems used. The pressures and temperatures presented correspond to the cycle points in Figure 1.

Parameter	Case I	Case II	Case III
T_{hot}		450 °C	
p_{back}		1.15 bar	
x_{NH_3}	0.3	0.65	0.65
$n_{aux,cold}$	0	0	2
p_2	19.84 bar	28.67 bar	28.67 bar
p_E	9.22 bar	19.85 bar	19.81 bar
T_E	429.17 °C	433.40 °C	434.30 °C
p_F	4.83 bar	4.44 bar	2.55 bar
η_{round}	23.56%	45.60%	59.38%
$w_{CH,compressor}$	752.94 kJ kg	851.57 kJ kg	851.57 kJ kg
$w_{DI,turbine}$	177.75 kJ kg	390.16 kJ kg	507.97 kJ kg

parameters and results are shown in **Table 1**, the *T*–*s* diagrams are shown in **Figure 11**.

The diagrams of case I (Figure 11a) and II (Figure 11b) show a poor thermal match between the charge and discharge cycle. Furthermore, the curvature at $x_{NH_3} = 0.3$ in case I is more pronounced than for $x_{NH_3} = 0.65$ in case II, which leads to even higher entropy generation in the heat exchangers and therefore higher losses in round-trip efficiency. This is particularly important on the hot side, as a better thermal match can only be influenced by the ammonia mass fraction. The better thermal match leads to a higher discharge turbine entry temperature T_E, as shown in Table 1. Due to the change in composition, the charge

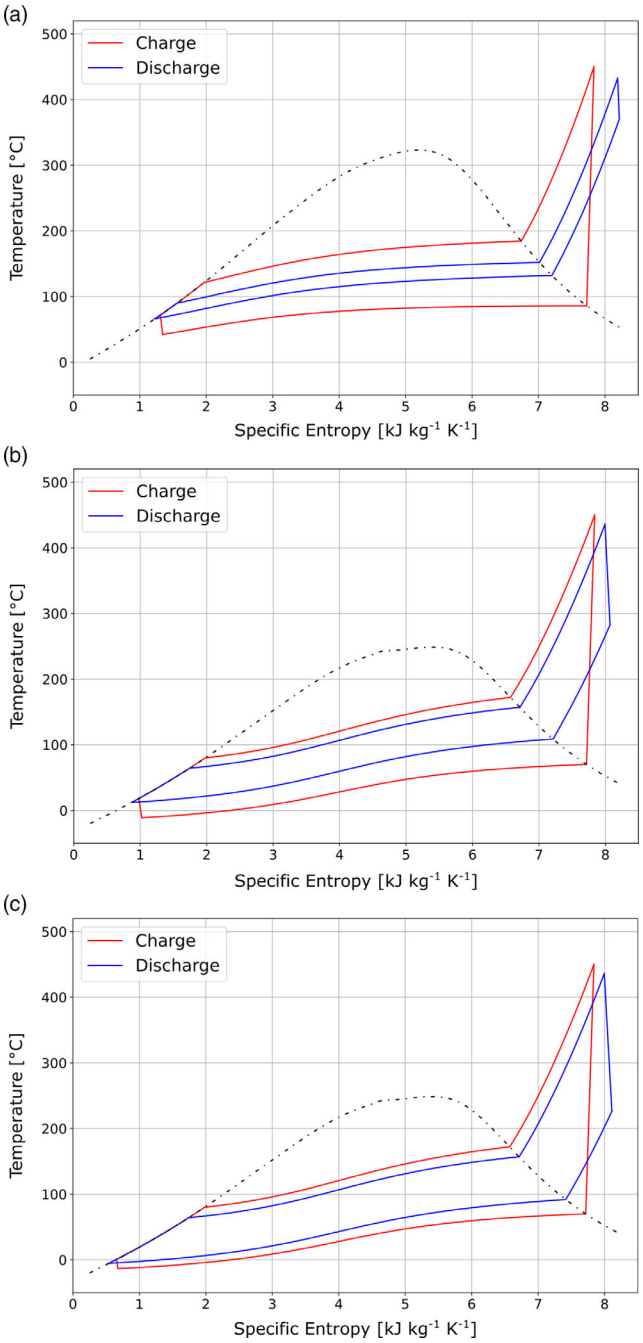

Figure 11. *T*–*s* diagrams for three different parameter sets as stated in Table 1. a) corresponds to Case I, b) to Case II, and c) to Case III. A close graphical match of the charging and discharging cycles implies a high round-trip efficiency. For such a match to occur, the design team needs to choose the operating parameters with care.

compressor and discharge turbine work both increase, but with a different ratio, which increases the round-trip efficiency significantly. Further improvements can be made by adding cold-side auxiliary storage systems, as shown in Figure 5. Although the charge cycle stays objectively the same in case II and III (Figure 11c), the discharge turbine can now discharge to a much

lower pressure, represented here by p_F. This again leads to a significantly higher round-trip efficiency. The working fluid states for all three cases and a high-efficiency case that captures further improvements can be found in the Appendix.

As the simulation calculates the working fluid state, and therefore the entropy, in every point of both cycles (Section 2.4), the entropy generation for the different machines can be calculated. The results for case I and III are shown in **Figure 12**. The entropy generation in the heat exchangers, particularly on the cold side, dominate the entire system. Even though the absolute entropy generation in case III is about 45% lower than in case I, the entropy generation in the heat exchangers still make up roughly 73% of the remaining total, highlighting the significance of these components.

In **Figure 13**, the Pareto front of the achievable volumetric expander work, i.e., the enthalpy change in (E→F) multiplied by the working fluid density ρ_i at the expander inlet in point E, is plotted against the ammonia mass fraction x_{NH_3} for all simulations. The graph suggests that higher fractions of ammonia in the mixture lead to higher volumetric expander work and thus to smaller machines for a given power production. Therefore, choosing a higher ammonia mass fraction leads to smaller machinery and thus lower investment cost. Coupled with the peak efficiency of a given system at about 65% ammonia mass fraction, the choice of composition of the working fluid is rather straightforward. The question about the amount of cold-side auxiliary storage systems used and the ceiling temperature targeted becomes an economical consideration. As more storage units and higher temperatures allow for higher round-trip efficiency, the added investment and operating cost for more and better machinery needs to be weighed against the expected returns.

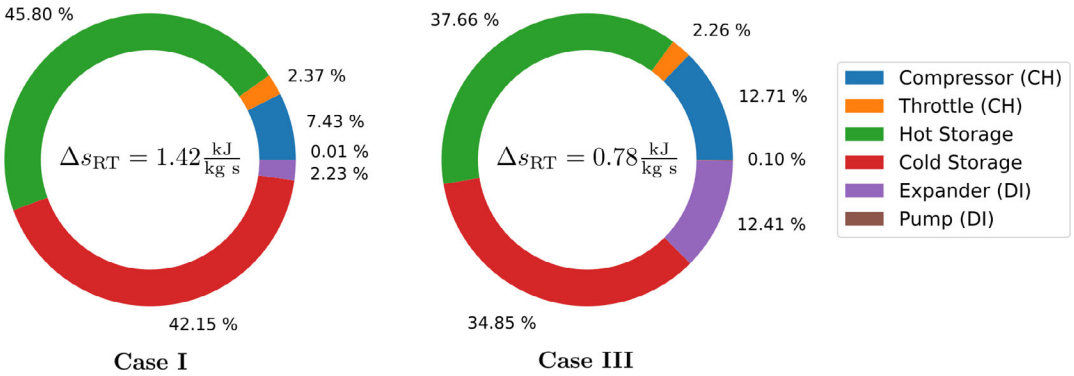

Figure 12. Entropy generation for cases I and III in Figure 11. Losses from the pump are so small that they are not visible in these diagrams. The entropy generation in the heat exchangers dominates the entire system's loss inventory, so that a small pinch point temperature approach ΔT_{pinch} and numerous auxiliary storage systems ($n_{aux,cold}$) should be considered during system design.

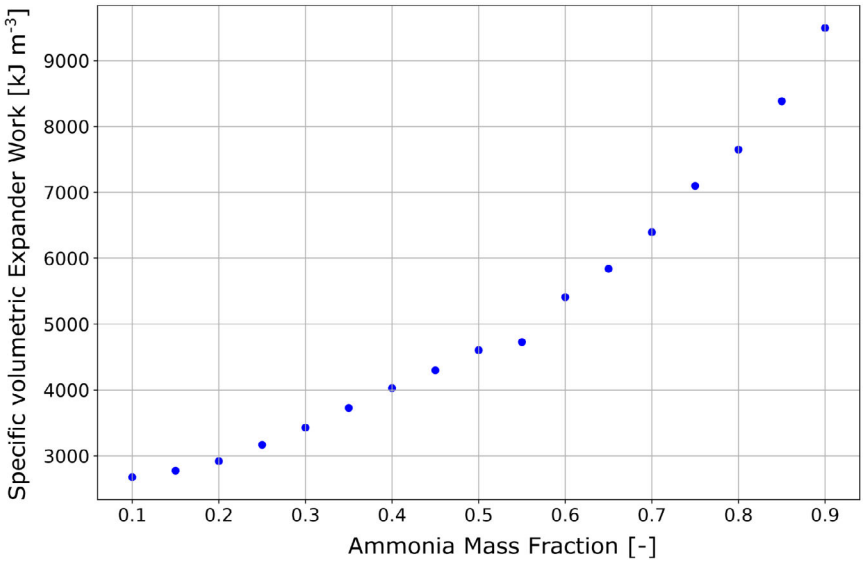

Figure 13. The Pareto front of the volumetric expander work extracted for different values of ammonia mass fraction shows that higher concentrations of ammonia lead to more mechanical energy being extracted from each volume of working fluid. This is important to estimate sizing of the machinery. Working fluids with a higher energy density allow for smaller machinery, which in turn decreases investment cost.

3.3. Detailed Impact on Round-Trip Efficiency

To understand the influence that the different components have on the storage system round-trip efficiency, 30 000 simulations were run with a random selection of parameters according to **Table 2**. The impact each of these parameters has on round-trip efficiency is shown in **Figure 14**. The distribution in each graph is modeled with a quadratic regression model and 95% prediction bands,[43] i.e., 95% of future observations are predicted to fall within the range between these two bands. The round-trip efficiency limits were chosen from 0 to 1 to show the full correlation between the individual parameters and η_{round}.

3.3.1. Gas Side Machines

While both graphs show a closely linear relationship, the impact of the charge compressor efficiency (Figure 14a) is slightly higher than that of the discharge expander (Figure 14b). Even though charge compressor losses are retained in the system as heat, the resulting loss in ceiling pressure seems to be of higher significance. Lower ceiling pressure leads to lower condensation temperature and to a higher curvature of the hot-side condensation and boiling stage thermal profile. In contrast, a lower expander efficiency leads to more waste heat being generated, but the achieved bottom pressure is always determined by the subsequent condenser.

3.3.2. Fluid-Side Machines

The fluid-side machines have less of an impact on round-trip efficiency than the gas side machines, as shown in Figure 14c, for the charge cycle liquid expander and in Figure 14d, for the discharge side pump. In fact, the fluid pump isentropic efficiency is of no importance to the round-trip efficiency. Nevertheless, care should be taken in choosing an appropriate pump, as parasitic effects from the motors, not modeled here, are expected to have an additional impact on the entire system's economics. The charge cycle throttle is of particular interest, as Figure 14c shows the effect of a hypothetical fluid side expander from an efficiency of 0 (regular throttle) to 0.95 (highly efficient fluid turbine). As the enthalpy contained in a unit of fluid pressurized to about 50 bar is minuscule compared with the enthalpy deposited in the same unit during gas side compression, the impact of a fluid expander for mechanical energy recuperation on the round-trip efficiency is negligible. The mean round-trip efficiency of a cycle with a fluid expansion turbine is only about 1.1 percentage-points higher than a cycle with a throttle that recuperates no mechanical energy. The choice of using an expansion turbine versus a throttle therefore becomes an economic consideration with an expander probably only being utilized in the largest of possible storage systems to obtain a marginal efficiency advantage.

Table 2. These are the parameter bounds used to carry out 30 000 simulations with randomly different values for each parameter.

Parameter	Lower bound	Upper bound
$\eta_{\text{CH,Comp.}}$	0.85	0.95
$\eta_{\text{DI,Exp.}}$	0.85	0.95
$\eta_{\text{CH,Exp.}}$	0.00	0.95
$\eta_{\text{DI,Pump}}$	0.75	0.95
T_{hot} [°C]	450	500
p_{back} [bar]	0.5	1.5
Δp [kPa]	5	55
ΔT_{pinch} [K]	1	10
$n_{\text{aux,cold}}$	1	3

3.3.3. Heat Exchangers

The impact of the heat exchanger pressure drop is shown in Figure 14e. Unsurprisingly, a larger pressure drop leads to a lower average round-trip efficiency in the storage system. This is due to a higher entropy generation in the heat exchangers and a resulting higher temperature spread between the charge and discharge cycle thermal streams. This would suggest that care should be taken to minimize the pressure drop by choosing heat exchangers with a large hydraulic cross section. Unfortunately, the heat exchanger pinch point temperature approach ΔT_{pinch} has an outsize impact on the system's round-trip efficiency for the proposed cycle layout, as shown in Figure 14f. Larger pinch points lead to even more entropy generation in the heat exchangers, such that an increase in ΔT_{pinch} by as little as 1 K can lead to a round-trip efficiency loss of 3 percentage-points. For $\Delta T_{\text{pinch}} \geq 9\,\text{K}$, no simulation resulted in a round-trip efficiency greater than 60%. The pinch point temperature difference is therefore a paramount parameter in designing the entire storage system. Compact heat exchangers, such as printed circuit heat exchangers (PCHE), enable stream temperature approaches as close as 1 K.[40] However, this again becomes an economic consideration, as small pinch points lead to large heat exchangers and, thus, to higher investment costs. Furthermore, PCHE have a small hydraulic cross section to maximize their surface area, which leads to increased pressure losses. The appropriate choice of heat exchangers is therefore no trivial task and needs to be approached with care.

3.3.4. Back Pressure and Cold-Side Auxiliary Storage Systems

The influence of the charge cycle back pressure, which is provided by the user at the start of the simulation, is shown in Figure 14g. Contradictory to expectations, a lower back pressure does not lead to higher round-trip efficiency, even though the discharge expander can expand to a lower pressure and thus extract more work from the working fluid. It seems that the additional work needed by the charge compressor more than offsets the aforementioned advantage. Furthermore, a lower back pressure leads to a stronger curvature of the working fluid thermal profile during cold-side evaporation and condensation, which, in turn, leads to a poorer thermal match and higher entropy generation in the cold-side heat exchanger. The advantages level off at about $p_{\text{back}} = 1.6\,\text{bar}$ for the proposed cycle layout.

Finally, in Figure 14h, the impact of adding additional auxiliary storage systems is shown. Using three or more auxiliary storage units, the system's round-trip efficiency can be increased

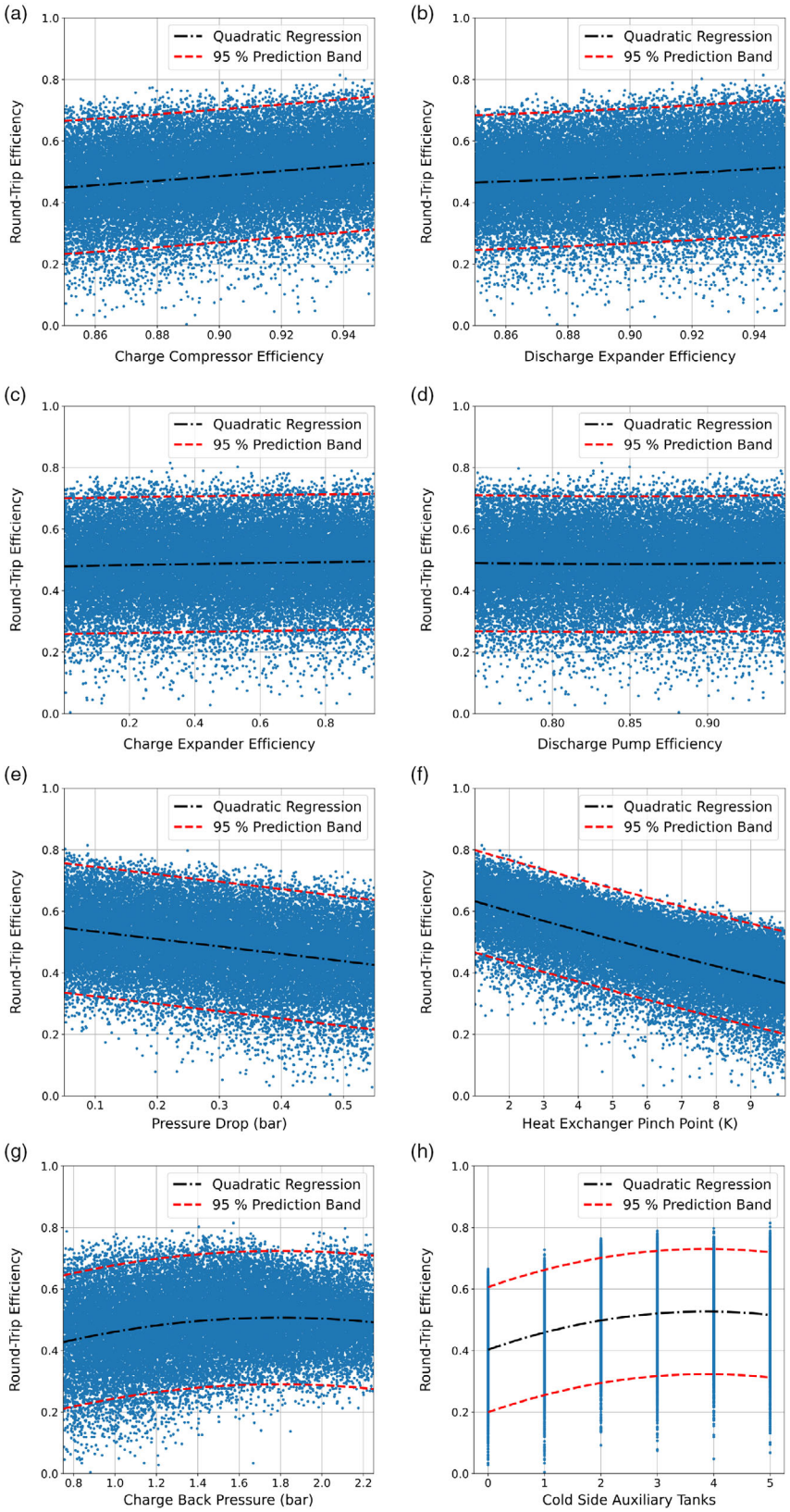

Figure 14. Displayed are the results for 30 000 simulations for different parameter combinations, as shown in Table 2. The graphs a)–h) show the impact each parameter has on the storage system round-trip efficiency, with prediction bands providing statistical context.

by as much as 15 percentage-points in comparison with having no auxiliary storage tanks. As discussed earlier, this is due to the better matching of the cold-side charge, storage, and discharge streams and the resulting minimization of entropy losses. This positive effect is clearly finite, which is why no more than five auxiliary tanks have been simulated here. Without any auxiliary tanks, the round-trip efficiency is limited to less than 70% for all simulated cases. Overall, the amount of auxiliary storage tanks needs to be economically optimized together with the heat exchangers used.

3.4. Comparison with Other PTES Systems

As previously noted, there are a variety of PTES concepts available in the literature.

The technology developed and presented by Laughlin[8] uses nitrogen or air in a Brayton cycle. The system, as presented, has an efficiency of 57.3%, with highly efficient gas turbines and compressors and uses existing heat storage materials, e.g., molten salt, available in the industry today. As Steinmann et al.[16] point out, the efficiency of the technology drops significantly with a minor decrease in turbine or compressor performance, as the entire system has to be finely tuned to a design point. Also, the system requires an internal gas–gas heat exchanger with very low approach temperatures, which may significantly raise cycle cost.

Mercangöz et al.[12] developed a Rankine-based system that uses CO_2 at cycle pressures of up to 200 bar, but with a temperature limit of 180 °C. Morandin et al.[38] showed that a system efficiency of 62.3% can be reached with the heat exchanger pinch point of $\Delta T_{\text{pinch}} = 4$ K. The system uses water as sensible and ice as a latent heat thermal storage system, which lead to low storage cost. Due to the small temperature spread between the hot and cold side, the size of the thermal storage systems needs to be rather large.[16] Furthermore, a small decrease in heat exchanger performance leads to a significant loss of round-trip efficiency.

The water-based system developed by Steinmann[15] is probably the most ambitious, yet underdeveloped, concept published to date. The technology uses an ammonia bottom charge cycle, a six-stage compressor with fivefold intercooling to bring the water vapor to the appropriate temperature during charging, and relies on a $NaNO_3$ phase-change material latent heat storage system that has yet to be used in an industrial setting. In contrast, the system shows a high round-trip efficiency of over 70% with only small losses from large heat exchanger pinch points (ΔT_{pinch}) or sub-par compressors or turbines. Nevertheless, significant research is needed for machines, heat exchangers, and storage systems to further develop this technology.

In contrast, ZeoPTES shows many of these concepts' positive attributes with fewer drawbacks. With proper engineering, a round-trip efficiency in excess of 70% and even close to 80% can be achieved, with a single compression step that does not require intercooling. ZeoPTES solely relies on sensible storage materials, such as molten salt and pressurized water, as can be found in industry today. Furthermore, the system round-trip efficiency is comparatively resilient to a drop in turbine or compressor efficiency. Consequently, ZeoPTES requires careful engineering of the heat exchangers and works most efficiently when several auxiliary storage units are integrated into the system.

4. Conclusion

ZeoPTES, a PTES concept using a zeotropic mixture of ammonia and water as working fluid was introduced. As the system uses a Rankine cycle, it is characterized by a low back work ratio during charging and discharging, which is beneficial for the round-trip efficiency. The use of a zeotropic mixture allows utilizing sensible storage units in all parts of the system, as evaporation and condensation of the working fluid are not isothermal. Therefore, thermal storage systems like pressurized water or molten salt, which are standard in industry today, may be employed. A simulation of the proposed cycle was written and the impact of different cycle parameters analyzed. A mass concentration of 65% of ammonia in water yielded the best results.

Losses in round-trip efficiency arise due to irreversible state changes in the heat exchangers and working machines. From Section 3, it is apparent, that the greatest loss-generator is the thermal storage systems. Their impact can be somewhat reduced with the use of multiple cold-side auxiliary storage tanks during condensation and evaporation, as outlined in Section 2.3. These allow for a better match of the storage system thermal energy stream with the working fluid stream and have a particularly large impact on the storage system cold side, where the curvature of the thermal streams of the working fluid is most pronounced due to the low pressure. Furthermore, the use of heat exchangers with small pinch points, such as PCHE, could improve efficiency. In Section 3.3, it was shown that the pinch point temperature approach ΔT_{pinch} has the highest impact on system round-trip efficiency of all the parameters analyzed. Further increases in efficiency may be obtained using gas-side working machines, i.e., compressors and expanders, with high internal isentropic efficiency, whereas the compressor is the more important of the two. Simulations using viable system parameters were able to achieve a round-trip efficiency of over 70% with individual simulations reaching over 80% for highly efficient working machines and extremely low heat exchanger pinch points.

This analysis of ZeoPTES focuses on a high power-to-power round-trip efficiency, as the storage of electricity is considered critical for the future build-out of renewable energy. Nevertheless, the graphs shown in Section 3.1 and 3.2 show waste heat generated at temperatures of 150–250 °C, a temperature level that is attractive for use in industrial applications. Subsequent work will not only focus on round-trip power-to-power efficiency, but will also account for investment and operating cost as well as potential revenue streams from the sale of electricity and industrial heat. Such an analysis will need to compare standard shell-and-tube with comparatively uncommon microchannel heat exchangers.

Furthermore, a multistep compression with intermediate cooling could allow for a higher hot-side pressure to be reached. That may lead to a smaller dependency on the number of auxiliary storage systems and a lower impact of the heat exchanger pinch point temperature difference. Finally, future work will also investigate whether heating from and cooling to the environment

may be a viable alternative to mitigate the issues arising from the strong curvature of the cold side working fluid thermal profile. The combination of different approaches might drive down investment costs which could lead to economically viable, large-scale energy storage systems.

Appendix

Depicted in the following tables are the state points for cases I, II, and III covered in Section 3.2, as well as a high-efficiency cycle layout. The input parameters used are given in the table descriptions (**Table A1**, **A2**, **A3**, and **A4)**.

Table A1. State points for case I. $x_{NH_3} = 0.3$, $T_{hot} = 450\,^{\circ}C$, $p_{back} = 1.15$ bar, $\Delta T_{pinch} = 3$ K, $\Delta p = 0.3$ bar, $n_{aux,cold} = 0$, $\eta_{CH,Comp.} = \eta_{DI,Exp.} = 0.9$, and $\eta_{round} = 23.56\%$.

State	p [bar]	T [°C]	h [kJ kg^{-1}]	s [kJ kg^{-1} K^{-1}]
1	1.15	93.90	2468	7.62
2	19.85	450.00	3221	7.73
3	19.55	194.30	2594	6.66
4	19.25	132.42	559	2.10
5	18.95	77.91	291	1.39
6	1.45	48.40	291	1.43
A	4.53	71.87	260	1.31
B	10.12	71.93	261	1.31
C	9.82	101.36	405	1.71
D	9.52	163.41	2568	6.91
E	9.22	429.17	3185	8.03
F	4.83	349.39	3007	8.06

Table A2. State points for case II. $x_{NH_3} = 0.65$, $T_{hot} = 450\,^{\circ}C$, $p_{back} = 1.15$ bar, $\Delta T_{pinch} = 3$ K, $\Delta p = 0.3$ bar, $n_{aux,cold} = 0$, $\eta_{CH,Comp.} = \eta_{DI,Exp.} = 0.9$, and $\eta_{round} = 45.60\%$.

State	p [bar]	T [°C]	h [kJ kg^{-1}]	s [kJ kg^{-1} K^{-1}]
1	1.15	77.27	2145	7.61
2	28.67	450.00	2996	7.73
3	28.37	181.05	2277	6.49
4	28.07	90.84	492	2.14
5	27.77	23.41	141	1.07
6	1.45	−5.93	141	1.12
A	4.14	17.31	107	0.97
B	20.75	17.51	110	0.97
C	20.45	75.62	412	1.92
D	20.15	167.13	2270	6.62
E	19.85	433.40	2961	7.85
F	4.44	270.40	2571	7.93

Table A3. State points for case III. $x_{NH_3} = 0.65$, $T_{hot} = 450\,^{\circ}C$, $p_{back} = 1.15$ bar, $\Delta T_{pinch} = 3$ K, $\Delta p = 0.3$ bar, $n_{aux,cold} = 2$, $\eta_{CH,Comp.} = \eta_{DI,Exp.} = 0.9$, and $\eta_{round} = 59.38\%$.

State	p [bar]	T [°C]	h [kJ kg^{-1}]	s [kJ kg^{-1} K^{-1}]
1	1.15	77.27	2145	7.61
2	28.67	450.00	2996	7.73
3	28.37	181.05	2277	6.49
4	28.07	90.84	492	2.14
5	27.77	6.79	54	0.77
6	1.45	−8.02	54	0.79
A	2.25	0.68	20	0.66
B	20.71	0.87	22	0.66
C	20.41	75.53	361	1.91
D	20.11	167.04	2220	6.62
E	19.81	434.30	2913	7.86
F	2.55	219.52	2405	7.98

Table A4. State points for a high-efficiency layout. $x_{NH_3} = 0.65$, $T_{hot} = 500\,^{\circ}C$, $p_{back} = 1.7$ bar, $\Delta T_{pinch} = 2$ K, $\Delta p = 0.1$ bar, $n_{aux,cold} = 5$, $\eta_{CH,Comp.} = \eta_{DI,Exp.} = 0.92$, and $\eta_{round} = 75.00\%$.

State	p [bar]	T [°C]	h [kJ kg^{-1}]	s [kJ kg^{-1} K^{-1}]
1	1.70	87.13	2163	7.48
2	55.62	500.00	3110	7.58
3	55.52	210.27	2270	6.20
4	55.42	130.05	709	2.69
5	55.32	8.26	64	0.79
6	1.80	-3.26	64	0.82
A	2.54	3.85	36	0.72
B	46.55	4.31	43	0.72
C	46.45	118.86	645	2.53
D	46.35	202.22	2276	6.29
E	46.25	482.48	3069	7.61
F	2.64	176.69	2357	7.75

Acknowledgements

Open access funding enabled and organized by Projekt DEAL.

Conflict of Interest

The author declares no conflict of interest.

Data Availability Statement

The data that support the findings of this study are available from the corresponding author upon reasonable request.

Keywords

carnot batteries, electrothermal energy storages, pumped thermal energy storages, zeotropic working fluids

Received: June 1, 2021
Revised: September 14, 2021
Published online:

[1] M. C. Lott, S.-I. Kim, C. Tam, D. Houssin, J. Gagné, Technology Roadmap: Energy Storage, **2014**, https://www.iea.org/reports/technology-roadmap-energy-storage, (accessed: February 2021).
[2] DOE Global Energy Storage Database, https://www.sandia.gov/ess-ssl/global-energy-storage-database-home, (accessed: April 2021).
[3] P. Das, B. K. Das, N. N. Mustafi, M. T. Sakir, *Energy Storage* **2021**, *3*, e223, https://doi.org/10.1002/est2.223.
[4] M. M. Rahman, A. O. Oni, E. Gemechu, A. Kumar, *Energy Convers. Manage.* **2020**, *223*, 113295.
[5] A. Benato, A. Stoppato, *Therm. Sci. Eng. Progr.* **2018**, *6* 301.
[6] R. B. Peterson, *Energy* **2011**, *36*, 6098.
[7] A. Thess, *Phys. Rev. Lett.* **2013**, *111*, 110602.
[8] R. B. Laughlin, *J. Renew. Sustain. Energy* **2017**, *9*, 044103.
[9] T. Desrues, J. Ruer, P. Marty, J. Fourmigué, *Appl. Therm. Eng.* **2010**, *30*, 425.
[10] J. Macnaghten, J. S. Howes, *Energy Storage* **2007**, *9*, 044103, GB0719259D0.
[11] T. R. Davenne, B. M. Peters, *Front. Energy Res.* **2020**, *8*, 160.
[12] M. Mercangöz, J. Hemrle, L. Kaufmann, A. Z'Graggen, C. Ohler, *Energy* **2012**, *45*, 407.
[13] M. Morandin, M. Mercangöz, J. Hemrle, F. Maréchal, D. Favrat, *Energy* **2013**, *58* 571.
[14] Y.-M. Kim, D.-G. Shin, S.-Y. Lee, D. Favrat, *Energy* **2013**, *49* 484.
[15] W.-D. Steinmann, *Energy* **2014**, *69* 543.
[16] W.-D. Steinmann, H. Jockenhöfer, D. Bauer, *Energy Technol.* **2019**, *8*, 1900895.
[17] H. Jockenhöfer, W.-D. Steinmann, D. Bauer, *Energy* **2018**, *145*, 665.
[18] A. H. Hassan, L. O'Donoghue, V. Sánchez-Canales, J. M. Corberán, J. Payá, H. Jockenhöfer, *Energy Rep.* **2020**, *6*, 147.
[19] B. Eppinger, L. Zigan, J. Karl, S. Will, *Appl. Energy* **2020**, *280*, 115940.
[20] B. Eppinger, D. Steger, C. Regensburger, J. Karl, E. Schlücker, S. Will, *Appl. Energy* **2021**, *288*, 116650.
[21] W.-D. Steinmann, D. Bauer, H. Jockenhöfer, M. Johnson, *Energy* **2019**, *183* 185.
[22] O. Dumont, G. F. Frate, A. Pillai, S. Lecompte, M. D. Paepe, V. Lemort, *J. Energy Storage* **2020**, *32*, 101756.
[23] B. M. Fronk, S. Garimella, *Int. J. Heat Mass Transfer* **2016**, *101*, 1343.
[24] B. M. Fronk, S. Garimella, *Int. J. Heat Mass Transfer* **2016**, *101*, 1357.
[25] A. I. Kalina, *J. Eng. Gas Turbines Power* **1984**, *106*, 737.
[26] A. I. Kalina, H. M. Leibowitz, in *Volume 3: Coal, Biomass And Alternative Fuels; Combustion And Fuels; Oil And Gas Applications; Cycle Innovations*. American Society of Mechanical Engineers, NewYork, NY **1988**.
[27] H. Leibowitz, M. Mirolli, *Power Eng.* **1997**, *101*, 44.
[28] M. Mirolli, H. Hjartarson, H. A. Mlcak, M. Ralph, *Operat. Maint. Mater. Issues* **2002**, *1*, 2.
[29] A. Modi, F. Haglind, *Appl. Therm. Eng.* **2015**, *76*, 196.
[30] E. Batuecas, C. Mayo, R. Daz, F. Pérez, *Sol. Energy Mater. Sol. Cells* **2017**, *171*, 91.
[31] R. W. Bradshaw, N. P. Siegel, in *ASME 2008 2nd Int. Conf. on Energy Sustainability, Volume 2*, Jacksonville, FL, USA **2008**.
[32] J. Howes, *Proc. IEEE* **2012**, *100*, 493.
[33] C. Willich, A. White, *J. Energy Storage* **2017**, *14*, 322.
[34] A. J. White, G. Parks, C. N. Markides, *Appl. Therm. Eng.* **2013**, *53*, 291.
[35] A. J. White, *Appl. Energy* **2011**, *88*, 4150.
[36] F. Sorgulu, I. Dincer, *Int. J. Energy Res.* **2018**, *43*, 6151.
[37] H. D. Baehr, S. Kabelac, *Thermodynamik - Grundlagen Und Technische Anwendungen*, 15 ed., Springer Vieweg, Berlin **2012**.
[38] M. Morandin, F. Maréchal, M. Mercangöz, F. Buchter, *Energy* **2012**, *45*, 375.
[39] M. Morandin, F. Maréchal, M. Mercangöz, F. Buchter, *Energy* **2012**, *45*, 386.
[40] F. Pra, P. Tochon, C. Mauget, J. Fokkens, S. Willemsen, *Nucl. Eng. Des.* **2008**, *238*, 3160.
[41] I. H. Bell, K. Gao, J. Wu, E. W. Lemmon, A Helmholtz-Energy Equation of State for Ammonia + Water, Unpublished.
[42] M. Huber, A. Harvey, E. Lemmon, G. Hardin, I. Bell, M. McLinden, NIST Standard Reference Database 23: Reference Fluid Thermodynamic and Transport Properties-REFPROP, Version 10.0, National Institute of Standards and Technology **2018**, https://www.nist.gov/srd/refprop (accessed: September 2021).
[43] S. M. Ross, *Introductory Statistics*, 4th ed., Academic Press, San Diego, CA **2017**.